# MRI Denoise and Deblur

Răzvan Stancu
BIOSINF

***Abstract*—Magnetic Resonance Imaging (MRI) is a common medical imaging technique used to produce detailed images of the internal body structures, especially soft tissues like the brain. It works by using strong magnets and radio waves, making it very useful for diagnosing a range of medical conditions. Despite its effectiveness, MRI images can sometimes become blurred or noisy due to patient movement, technical limitations, or other environmental factors. These imperfections can significantly affect the accuracy of diagnoses, posing serious problems in medical settings. This paper explores different deep learning techniques designed to reduce blur and noise in MRI images. The models are trained using datasets that have been intentionally blurred and noised, allowing them to learn how to restore clear and accurate images. Their performance is tested on a completely new set of MRI images, ensuring the results reflect their real-world applicability. Additionally, we compare these deep learning methods with a classical computer vision algorithm to see how they measure up. The paper covers the latest methods in the field, the data used for experiments, details about the experimental setup, and an analysis of the findings. Finally, conclusions are presented along with references for further reading.**

## I. State of the art

MRI scans often serve as the first step in the diagnosis of a wide range of conditions, so a certain quality must be maintained to allow the medics to perform their job properly. However, the quality of these scans is frequently compromised by blur and noise, which can be introduced by a variety of sources. One common issue is patient movement during the scan, often unavoidable and difficult to control, which leads to motion blur. Additionally, hardware limitations and a low signal-to-noise ratio can further degrade the image. These imperfections can obscure important anatomical details, potentially leading to missed diagnoses or misinterpretations. Therefore, improving the clarity of MRI scans is crucial for ensuring accurate medical assessments.

To address these challenges, researchers have developed a wide range of techniques aimed at restoring image quality. These methods focus on two main goals: denoising, which targets the removal of unwanted random fluctuations in the image, and deblurring, which seeks to recover sharpness lost during acquisition. Generally, solutions fall into two major categories: traditional algorithmic techniques and deep learning-based approaches. The following sections review notable contributions in both domains, emphasizing their strengths, limitations, and relevance to MRI image restoration.

### A. Traditional Methods

Traditional image restoration methods are based on mathematical models and optimization algorithms. One well-known approach is Total Variation (TV) minimization, which preserves edges while reducing noise. Another class involves wavelet-based denoising, such as the SureShrink method [1], which adapts thresholding to the wavelet coefficients. Non-local means (NLM) filtering [2], another effective method, works by averaging similar patches across the image, maintaining structural information.

MRI images are commonly affected by Additive White Gaussian Noise (AWGN), characterized by its normal distribution and statistical independence from the signal. Gaussian filters, which apply a smoothing kernel based on the Gaussian function, are often used to reduce this type of noise by averaging pixel values with their neighbors. However, while Gaussian filters are computationally simple, they tend to blur edges and fine details.

Another frequent noise type in MRI, especially in magnitude images, is Rician noise. This type of noise arises due to the nature of MRI acquisition and reconstruction processes and is more complex than Gaussian noise. Traditional denoising methods for Rician noise often rely on variance-stabilizing transformations (e.g., the Anscombe transform) or specialized models that consider the signal-dependent nature of the noise.

For deblurring, classic iterative methods like the Richardson-Lucy deconvolution [3], [4] and Wiener filtering [5] have been widely applied. These methods often assume that the blur kernel is known, which might not always be available. Fourier transform-based methods are also commonly used, leveraging the convolution theorem to perform deblurring in the frequency domain, which can simplify the process but also introduce artifacts if noise is not managed. While effective under certain conditions, traditional methods often require careful tuning and assumptions about noise statistics or blur kernels, limiting their general applicability in clinical practice.

### B. Deep Learning Methods

In recent years, deep learning has revolutionized the field of image restoration. One of the most influential models is DnCNN [6], which uses convolutional layers and residual learning to remove Additive White Gaussian Noise (AWGN). Other methods like U-Net [7] and its variants have shown strong performance in both denoising and deblurring tasks, benefiting from their encoder-decoder structures and skip connections.

Multiple versions of Convolutional Neural Networks (CNNs) have been adapted to tackle noise and blur in MRI images. Residual networks, for instance, help mitigate vanishing gradient issues and allow deeper architectures to be trained effectively. Dilated CNNs expand the receptive field without increasing the number of parameters, making them useful for capturing larger context in noisy images. U-Net and its

extensions remain a cornerstone in medical image processing due to their ability to combine high-resolution features from early layers with deeper, abstract representations. Variants like Attention U-Net incorporate attention gates to highlight salient regions of the image, improving focus on areas affected by artifacts. These mechanisms help the model distinguish between informative structures and irrelevant noise.

Attention mechanisms have also been introduced in other architectures. For example, the Residual Attention Network (RAN) and Transformer-based models enhance denoising by modeling long-range dependencies across the image. These attention modules allow the network to weigh pixel relationships globally, which is particularly useful in handling spatially complex noise patterns. Models like RIDNet [8] use a multi-feature fusion strategy to address real-world noise, while MPRNet [9] employs a multi-stage architecture that progressively refines the image through successive restoration blocks.

Despite their success, deep learning methods are not without limitations. They often require extensive labeled data for training and significant computational resources. Generalization to unseen types of noise or blur remains a challenge. their ability to learn powerful and flexible representations makes them particularly promising for MRI image enhancement tasks.

## II. Methods and Datasets Description

### A. Dataset

The dataset used in this study is publicly available on Kaggle [10]. It contains clean MRI images of the brain, categorized into four classes: glioma, meningioma, pituitary tumor, and no tumor. In order to ensure a balanced dataset, we selected 2,500 images from each class, resulting in a total of 10,000 clean images.

These images were divided into three subsets: 6,000 images for training (60%), 2,000 images for validation (20%), and 2,000 images for testing (20%). The validation set is used to update the model's hyperparameters during training, while the test set is reserved.

To simulate real-world imaging conditions, artificial noise and blur were added to the clean images. This includes motion blur using pre-generated filters, as well as Additive White Gaussian Noise (AWGN). Specifically, additional noisy sets were created with Gaussian noise at standard deviations of 0.1), applied evenly across the dataset. This allowed us to test how different models perform across various noise intensities while maintaining class balance. For a better comparison we also tested on blurred images without AWGN.

To ensure consistency and improve model convergence, all images were first padded to maintain aspect ratio and then resized to 256×256 pixels. Subsequently, pixel intensities were normalized using a mean of 0.1781 and a standard deviation of 0.1976, computed from the clean training set. This processing step centers the data distribution and helps stabilize gradient updates during training.

Each data sample is transformed into a pair of grayscale image tensors—one noisy and one clean—through a sequence of processing steps including resizing, normalization, and tensor conversion. These tensor pairs serve as aligned inputs and targets for supervised learning.

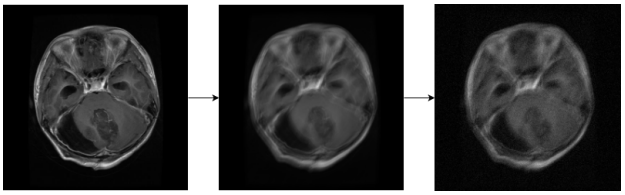

Fig. 1. Original Image to Motion Blur to Extra Noise

The transformation pipeline, illustrated in Figure 1, standardizes the data format and ensures that the neural network receives consistent, numerically stable input throughout the training process.

### B. Methods

To evaluate the effectiveness of different approaches for MRI image restoration, we implemented four deep learning models ranging from basic Convolutional Neural Networks (CNNs) to more advanced structures. These include a straightforward CNN, a U-Net model, an attention-based network, and a model tailored specifically for MRI denoising tasks. Each architecture was selected to represent a category of deep learning techniques.

In order to conduct a complete and fair comparison, a fifth method was also considered, an algorithmic technique for image restoration. This serves as a traditional baseline and allows for a practical evaluation of how deep learning methods outperform or complement handcrafted algorithms in noisy and blurred MRI scenarios.

Each one of the models was trained and tested under the same conditions to ensure consistency and fairness in evaluation.

DnCNN (Denoising Convolutional Neural Network), first introduced by Zhang [6], is built on the principles of residual learning and batch normalization, making it particularly well-suited for removing additive white Gaussian noise (AWGN). Rather than mapping noisy images directly to clean counterparts, DnCNN is trained to predict the noise residual—the difference between the noisy and clean image—which is then subtracted from the input to produce the denoised result. This formulation simplifies the learning task and supports the use of deeper networks. The original implementation consists of 17 convolutional layers using 3×3 kernels and 64 feature maps, with a receptive field of 35×35, balancing accuracy and computational cost.

DnCNN has become one of the most widely adopted architectures for image restoration, with researchers extending and adapting it across multiple domains beyond MRI and natural image denoising. For example, it has been successfully applied in hyperspectral image denoising, where the challenge is to suppress noise across both spatial and spectral dimensions. In these cases, DnCNN is often combined with spectral attention mechanisms or adapted to work in 3D to capture interband correlations. In deblurring applications, DnCNN has been used as a post-processing step in conjunction with classical

deconvolution techniques, improving the perceptual quality of deblurred images. Some works have also modified DnCNN by adding residual dense connections or attention gates, which make the network more aware of spatial context and help it adapt better to non-Gaussian or spatially variant noise. In biomedical imaging, DnCNN variants have been employed in fields such as ultrasound and CT denoising, showing that the core architecture generalizes well when retrained on domain-specific data. Its relatively lightweight design compared to more recent transformer-based models still makes DnCNN a go-to choice for tasks where computational efficiency and stability matter, especially in real-time or embedded settings.

In this work, DnCNN is the 2017 state-of-the-art configuration that also has incorporated additional training enhancements tailored to the MRI data. Additional metrics were added, SSIM and PSNR, on denormalized outputs to better capture perceptual quality. Chekpoints were also implemented for halting training if the validation MSE did not improve for five consecutive epochs while retaining the best-performing model. The chosen approach allows flexible batch sizing, with experiments including batches of up to 64 samples to stabilize training and accelerate convergence. Finally, to increase robustness, the network was trained using random AWGN

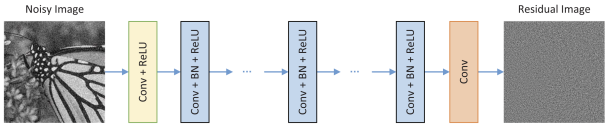


Fig. 2. DNCNN Architecture

CNN-DMRI is a specialized convolutional neural network designed to denoise MRI scans affected by Rician noise, a type of signal-dependent and non-additive noise commonly found in medical imaging. Unlike Gaussian noise, Rician noise presents greater challenges due to its complex statistical behavior, making traditional filtering methods less effective. To tackle this, CNN-DMRI uses a residual learning approach within an encoder-decoder architecture. The encoder extracts and compresses features from the noisy image, while the decoder reconstructs a denoised output by progressively recovering spatial detail. The network is trained to predict the noise component itself, which is then subtracted from the input image to produce a clean result. This residual strategy not only speeds up convergence but also enhances denoising accuracy.

Structurally, CNN-DMRI consists of multiple convolutional layers followed by downsampling operations that capture broader context, and then upsampling layers that rebuild the image. A global skip connection adds the predicted noise back to the input to form the final output. The model is trained end-to-end using MSE loss, and has been tested on both synthetic and real-world datasets across various anatomical regions. Evaluation metrics such as PSNR and SSIM show that CNN-DMRI performs better than classical methods like Non-Local Means and PCA-based denoising, particularly in more severe noise scenarios.

In practice, CNN-DMRI stands out for its balance between simplicity and performance. For our purposes, the architecture was reimplemented in PyTorch and adapted to handle 256×256 grayscale MRI images. While staying true to the original design, we made small adjustments to accommodate different noise levels and dataset formats. These changes allowed for better integration into our pipeline, while maintaining the model's core strength: learning robust denoising features tailored for MRI. CNN-DMRI serves as a solid, domain-aware baseline and could be extended further with attention layers or multi-scale features in future work.

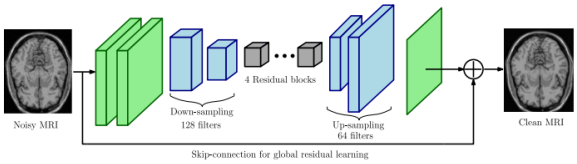


Fig. 3. CNN-DMRI Architecture

RIDNet (Residual-in-Residual Dense Network with Feature Attention) is an advanced deep learning model originally proposed for blind denoising of real-world images. It was developed in response to a common issue in denoising research: many CNN-based models are trained on synthetic noise, such as Gaussian noise, and tend to perform poorly when faced with real noise patterns that are more complex and variable. RIDNet is specifically designed to handle unknown and unstructured noise types without requiring prior estimation of noise levels, making it suitable for practical scenarios where noise characteristics are unpredictable.

The network architecture features a residual-on-residual structure that employs multiple shortcut connections, allowing the model to learn the residual noise more effectively while preserving low-frequency content. A key element in this design is the Feature Attention Module (FAM), which applies global average pooling followed by fully connected layers and a sigmoid activation to generate channel-wise attention maps. This recalibration mechanism enables the network to focus on the most informative features while suppressing irrelevant or noisy signals, particularly in high-detail regions where noise tends to blend with important structures.

RIDNet consists of an initial convolutional feature extractor, followed by a sequence of Enhancement Attention Modules (EAMs). Each EAM integrates residual blocks, dilated convolutions, and attention mechanisms to enhance feature learning across spatial scales. The final reconstruction layer assembles the denoised output. The original evaluation of RIDNet included comparisons with 19 leading denoising methods on synthetic and real-world datasets. Metrics such as PSNR and SSIM showed that RIDNet not only outperformed competitors numerically but also delivered superior visual quality, particularly under low-light conditions and in preserving fine textures.

For application to MRI denoising, the RIDNet architecture was adapted to accept single-channel grayscale inputs and anatomical slice sizes of 256×256 pixels. Training included simulated MRI noise distributions, including Rician noise, to align the model with domain-specific data characteristics. Despite being originally tailored for RGB natural images,

the residual design and attention-driven feature processing made RIDNet highly transferable to medical imaging contexts, demonstrating its value as a state-of-the-art approach for challenging denoising tasks.

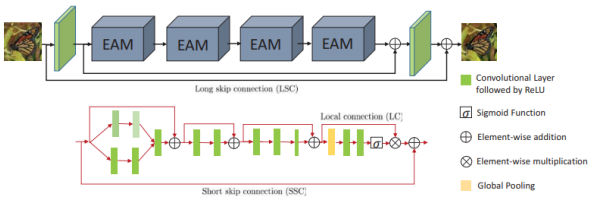


Fig. 4. RIDNET Architecture

The U-Net architecture, first introduced for biomedical image segmentation, has since become a foundational model in medical image processing tasks such as denoising and image reconstruction. It follows a fully convolutional encoder-decoder design, where the encoder progressively reduces spatial dimensions through convolution and pooling layers to extract high-level features, while the decoder restores the image to its original resolution through upsampling and convolutional reconstruction. A key strength of U-Net lies in its skip connections, which link corresponding layers in the encoder and decoder, allowing low-level spatial information to be directly reused during reconstruction. These connections help recover detail that may be lost during downsampling and are particularly effective in low-level tasks like denoising, where structural fidelity is essential.

In MRI denoising, U-Net's structure is especially beneficial due to its capacity to retain anatomical details while filtering out complex noise. The model's modularity has led to many variants tailored to different use cases, including Residual U-Net, Attention U-Net, and Dense U-Net. These extensions enhance specific aspects such as feature reuse, representation learning, or computational efficiency. U-Net's ability to combine context from multiple scales with precise spatial localization offers a clear advantage over simpler CNN-based architectures, particularly for medical imaging where both local textures and global anatomical context must be preserved.

The version used in this study is a streamlined implementation referred to as U-Lite, designed to maintain denoising performance while reducing computational complexity. U-Lite features a three-level encoder-decoder structure, with each stage composed of two 3×3 convolutional layers with ReLU activation, batch normalization, and residual shortcuts. Max pooling is used for downsampling in the encoder, while transposed convolutions perform upsampling in the decoder. Skip connections link matching encoder and decoder levels to retain spatial precision, and residual blocks in the decoder stages help refine reconstruction. A final 1×1 convolution produces the output denoised image.

This configuration operates on 256×256 grayscale MRI slices and outputs denoised images of the same resolution. While simpler than some alternatives such as CNN-DMRI or RDUNet, U-Lite retains the core strengths of U-Net, striking a balance between performance and efficiency. The model was trained using mean squared error (MSE) loss, offering a strong and interpretable baseline for MRI denoising tasks. It provides a reliable framework for deployment in time-sensitive or resource-constrained environments, and serves as a foundation that could be extended in future work with techniques like perceptual loss or attention modules.

The last method that this paper implemented is Richardson–Lucy algorithm is a widely used classical approach for image deblurring, especially in scenarios where the blur kernel—or point spread function (PSF) is known or can be estimated. Based on an iterative maximum likelihood estimation under Poisson noise assumptions, the RL algorithm updates the estimated image by comparing it to the observed blurred image, correcting it step by step. Each iteration refines the image using information from the PSF, allowing the method to progressively sharpen the degraded content. This iterative nature makes RL particularly suitable for controlled deblurring tasks where the noise model and blur characteristics are well-defined. However, the algorithm is also sensitive to noise and may introduce artifacts if too many iterations are used, especially in low signal-to-noise conditions, such as those found in MRI scans.

In this study, the RL algorithm was implemented as a benchmark method to provide a traditional, algorithmic baseline for comparison with deep learning-based solutions. It was applied to synthetically blurred MRI slices, where the blur kernel was predefined and consistent across samples. The number of iterations was empirically tuned to balance between detail recovery and noise amplification. Unlike data-driven approaches, RL does not rely on training data or learned features—it directly applies mathematical modeling to recover structure. While this limits its adaptability to complex, real-world degradations, it remains a useful tool for evaluating restoration performance under known degradation settings. Including RL in the evaluation framework highlights the strengths of learning-based methods, particularly in handling more diverse and less predictable image corruptions.

## III. Experiments and Results

All models were evaluated under a unified and fully reproducible experimental pipeline. Each denoising architecture—whether DnCNN, CNN-DMRI, RIDNet, or a lightweight U-Net variant—was trained and tested following the same sequence: preprocessing, training with early stopping, validation using perceptual and error-based metrics, and final evaluation on an unseen test set. All MRI images were resized to $256X256$ pixels, converted to single-channel grayscale tensors, and normalized using dataset-specific mean and standard deviation values. The dataset was partitioned into 60% training, 20% validation, and 20% testing subsets, with class balance preserved across all splits.

Training was conducted using the Adam optimizer with a fixed learning rate, minimizing the MSE loss between the model output and the clean reference image. A maximum of 50 epochs was allowed, with early stopping enabled if the validation loss did not improve for five consecutive epochs. The best-performing model weights, based on the lowest

validation MSE, were retained for final testing. Performance was evaluated using three standard image quality metrics:

MSE quantifies the average squared pixel-wise difference between the predicted image $\hat{I}(i,j)$ and the ground truth $I(i,j)$, which can be seen in (1).

$$\text{MSE} = \frac{1}{MN}\sum_{i=1}^{M}\sum_{j=1}^{N}\left[I(i,j) - \hat{I}(i,j)\right]^2 \tag{1}$$

Lower MSE values indicate better pixel-level accuracy.

SSIM evaluates perceptual quality by considering luminance, contrast, and structure in the following formula.

$$\text{SSIM}(x,y) = \frac{(2\mu_x\mu_y + C_1)(2\sigma_{xy} + C_2)}{(\mu_x^2 + \mu_y^2 + C_1)(\sigma_x^2 + \sigma_y^2 + C_2)} \tag{2}$$

Where $\mu_x$, $\mu_y$ are the local means, $\sigma_x^2$, $\sigma_y^2$ are the variances, and $\sigma_{xy}$ is the covariance of image patches $x$ and $y$. SSIM values range from -1 to 1, with higher values indicating better structural preservation.

PSNR measures reconstruction fidelity in decibels is defined in (3).

$$\text{PSNR} = 10 \cdot \log_{10}\left(\frac{\text{MAX}_I^2}{\text{MSE}}\right) \tag{3}$$

Where $\text{MAX}_I$ is the maximum possible pixel value, typically 1.0 for normalized images. Higher PSNR values correspond to cleaner reconstructions.

Each model was evaluated on the test set using its best checkpoint. Average MSE, SSIM, and PSNR values were reported. Metric distributions were visualized using histograms to analyze consistency, and qualitative comparisons were illustrated using sample triplets of noisy, denoised, and clean MRI images. This comprehensive evaluation ensured a fair and transparent comparison across all models.

During the main training phase, all models were optimized using the Adam optimizer with a fixed initial learning rate. The objective function minimized the pixel-wise mean squared error (MSE) between the predicted output and the clean reference image. Validation MSE was continuously monitored throughout training. An early stopping strategy was employed, terminating the process if no improvement in validation performance was observed over five consecutive epochs. The model weights corresponding to the epoch with the lowest validation MSE were retained to prevent overfitting.

In selected configurations, a secondary fine-tuning stage was applied using the best-performing checkpoint from the primary training. This phase used a reduced learning rate to allow the model to correct subtle residual artifacts while preserving the stability of the learned parameters. Post-training, the optimal weights for each model were reloaded and used to generate predictions on the hold-out test set.

Denoising performance was quantitatively assessed by computing per-image values for MSE, Structural Similarity Index Measure (SSIM), and Peak Signal-to-Noise Ratio (PSNR). These metrics were aggregated to report both mean values and the full statistical distributions across the test set. MSE histograms revealed variance and the presence of high-error outliers, while SSIM and PSNR distributions offered complementary insight into structural preservation and visual fidelity. This structured combination of loss-based training, optional fine-tuning, and statistical analysis provided a reliable and comprehensive evaluation framework for all tested models.

Table I shows the average performance of each denoising model across three metrics: MSE, SSIM, and PSNR. CNN-DMRI and U-Net Lite obtained the lowest mean squared error values ($1.00 \times 10^{-3}$), indicating the highest pixel-wise accuracy. In contrast, DnCNN reported the highest MSE ($26.60 \times 10^{-3}$), suggesting less accurate reconstructions overall. RIDNet fell in between with an MSE of $5.50 \times 10^{-3}$, showing moderate numerical performance.

When comparing perceptual quality through SSIM, CNN-DMRI achieved the highest score (0.8357), with U-Net Lite closely following (0.8203). These results imply that both models were able to preserve structural and visual details effectively. DnCNN reached a moderate SSIM of 0.7066, while RIDNet scored significantly lower (0.3366), indicating weaker preservation of textures and fine structures.

PSNR values supported these findings. CNN-DMRI achieved the highest PSNR at 32.17dB, closely matched by U-Net Lite at 31.91dB, both reflecting strong noise suppression and clear reconstructions. RIDNet achieved 24.20dB, while DnCNN lagged with only 18.19dB, reflecting higher levels of residual noise in the output images.

Overall, the results suggest that CNN-DMRI and U-Net Lite offered the best balance of pixel accuracy and perceptual quality, making them the most effective methods in this comparison. RIDNet and DnCNN were less consistent, particularly in preserving structural details and achieving high perceptual similarity.

TABLE I
AVERAGE PERFORMANCE METRICS FOR EACH DENOISING MODEL

| **Metric** | **CNN-DMRI** | **DnCNN** | **RIDNet** | **U-Net Lite** |
|---|---|---|---|---|
| MSE ($\times 10^{-3}$) | 1.00 | 26.60 | 5.50 | 1.00 |
| SSIM | 0.8357 | 0.7066 | 0.3366 | 0.8203 |
| PSNR [dB] | 32.17 | 18.19 | 24.20 | 31.91 |

Table II illustrates the distribution of SSIM scores across the test set for each of the four denoising models. CNN-DMRI and U-Net Lite exhibit the most concentrated and right-skewed distributions, with the majority of SSIM values falling between 0.8 and 0.95. This indicates consistent structural preservation and high perceptual quality across the dataset. DnCNN, while showing a more dispersed pattern, has its SSIM values centered around 0.7–0.8, reflecting moderate performance with more variation in output quality. RIDNet shows the weakest results, with a broad distribution peaking around 0.3–0.4 and extending into lower SSIM regions, suggesting difficulty in preserving structural features under noisy conditions. Overall, the histograms reinforce the numerical results from Table I, highlighting the superior consistency of CNN-DMRI and U-Net Lite in delivering perceptually coherent reconstructions.

Figure 5 provides a qualitative comparison of the denoising outputs produced by each model on a representative blurred MRI image. The noisy input, shown on the far left, appears visually degraded with noticeable smoothing and structural

TABLE II
SSIM DISTRIBUTIONS FOR EACH DENOISING MODEL ON THE TEST SET.

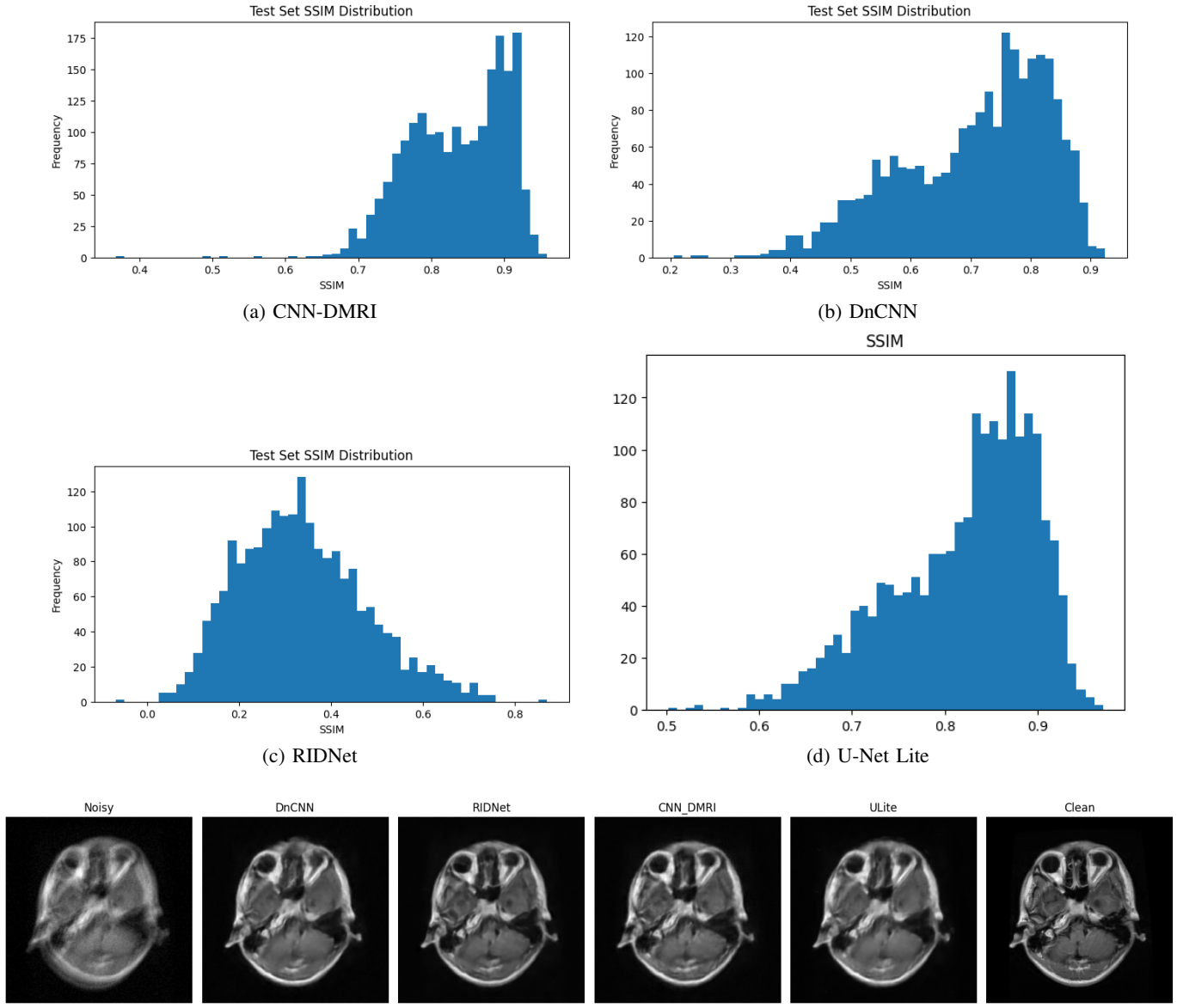


(a) CNN-DMRI (b) DnCNN (c) RIDNet (d) U-Net Lite

Fig. 5. Overview of all model's results on a blurred image.

loss. The reconstructions produced by CNN-DMRI and U-Net Lite show the highest visual fidelity, recovering fine anatomical details and closely resembling the clean reference image. DnCNN offers moderate reconstruction quality, although some features remain partially blurred. RIDNet's output appears less sharp and retains visible degradation, consistent with its lower SSIM and PSNR scores. Overall, the figure visually reinforces the quantitative metrics, demonstrating that CNN-DMRI and U-Net Lite are most effective at restoring structural integrity in blurred MRI data.

The results presented in this section correspond to the first experiment, where models were trained and evaluated on MRI images containing only synthetic blur, without the addition of any Gaussian noise. This setting establishes a baseline for performance under controlled, noise-free conditions and allows clearer assessment of each model's deblurring capability.

In the following experiment, the same test set was used to ensure consistent evaluation conditions. However, all models were retrained on data augmented with additive white Gaussian noise (AWGN) at a standard deviation of $\sigma = 0.1$. This setup simulates more challenging real-world scenarios where both blur and noise are present. The goal was to assess how well each architecture generalizes to combined distortions.

Table IV reports the average MSE, SSIM, and PSNR scores for each model when trained and evaluated in the presence of additive white Gaussian noise with $\sigma = 0.1$. Compared to the noise-free case in Table I, all models show a clear decline in performance across all metrics, reflecting the increased difficulty of the task. CNN-DMRI and U-Net Lite remain the top performers, with only slight increases in MSE (1.30 and

TABLE III
SSIM DISTRIBUTIONS UNDER AWGN ($\sigma = 0.1$) FOR EACH DENOISING MODEL.

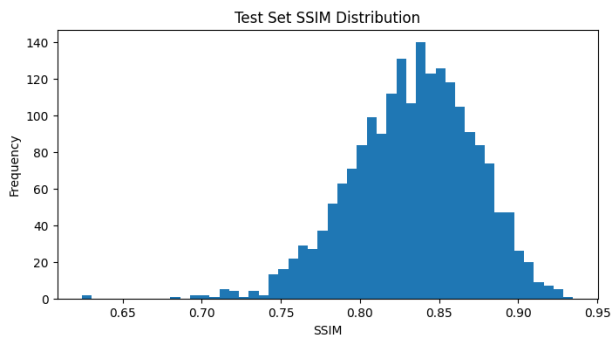


(a) CNN-DMRI

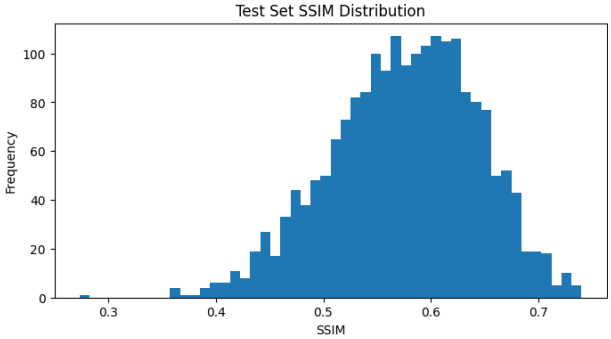


(b) DnCNN

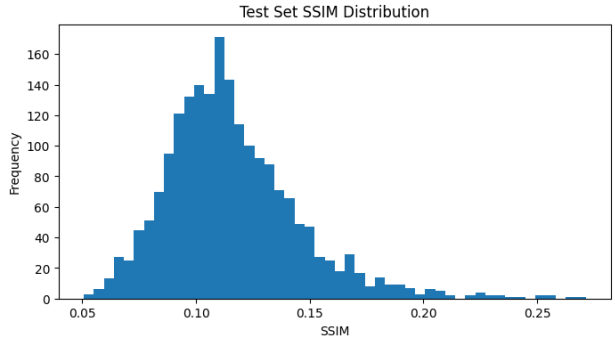


(c) RIDNet

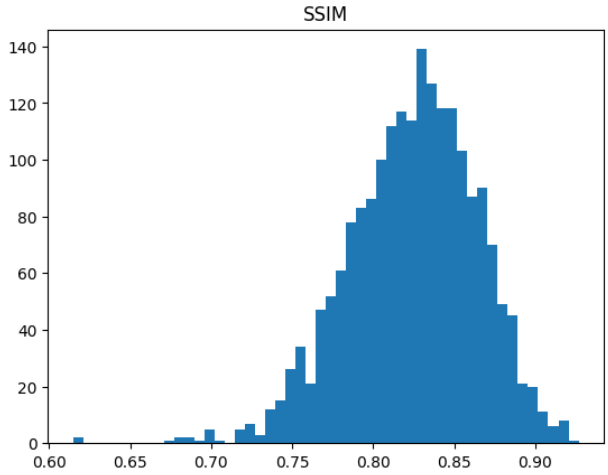


(d) U-Net Lite

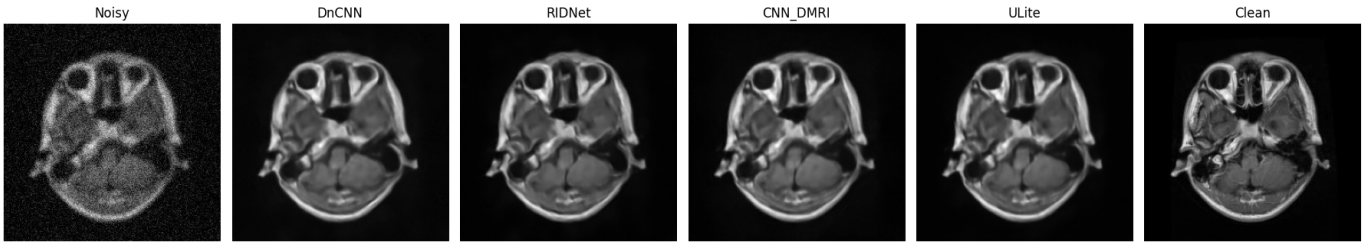


Fig. 6. Overview of all model's results on a blurred an image.

1.50 $\times 10^{-3}$ respectively) and minor drops in SSIM and PSNR, indicating robust generalization to noisy conditions.

DnCNN, on the other hand, exhibits a substantial performance drop, with MSE rising to 39.70 $\times 10^{-3}$ and SSIM decreasing to 0.5757. RIDNet performs particularly poorly in this setting, with a dramatic drop in SSIM to 0.1159 and a notable increase in error. These results suggest that CNN-DMRI and U-Net Lite are better suited for handling combined noise and blur, while DnCNN and RIDNet are more sensitive to noise corruption in MRI data.

Table III presents the SSIM distributions for each model when trained on data corrupted with AWGN at $\sigma = 0.1$. The histogram for CNN-DMRI (a) shows a strong concentration of SSIM values in the 0.80–0.90 range, indicating consistent and high structural preservation despite the added noise. U-Net Lite (d) shows a similar pattern, with a slightly broader spread but still centered around high SSIM values, confirming its robustness in noisy conditions. DnCNN (b) demonstrates a notable performance drop, with most SSIM values falling between 0.50 and 0.70 and a wider distribution overall. This reflects a reduced ability to maintain perceptual quality under noise. RIDNet (c) performs the worst, with SSIM values

TABLE IV
AVERAGE PERFORMANCE METRICS FOR EACH DENOISING MODEL UNDER AWGN ($\sigma = 0.1$).

| **Metric** | **CNN-DMRI** | **DnCNN** | **RIDNet** | **U-Net Lite** |
|---|---|---|---|---|
| MSE ($\times 10^{-3}$) | 1.30 | 39.70 | 15.90 | 1.50 |
| SSIM | 0.8336 | 0.5757 | 0.1159 | 0.8245 |
| PSNR | 29.24 | 14.43 | 18.03 | 28.78 |

heavily skewed toward the lower end (0.05–0.20), suggesting significant degradation in structural detail retention. These distributions support the quantitative metrics in Table IV, further emphasizing the superior resilience of CNN-DMRI and U-Net Lite to combined blur and Gaussian noise.

Figure 6 shows visual comparisons of the denoising outputs produced by each model when trained with AWGN ($\sigma = 0.1$). The noisy input image (far left) displays significant degradation, with both blur and high-frequency Gaussian noise obscuring anatomical structures. Among the restored images, CNN-DMRI and U-Net Lite again produce the clearest reconstructions, closely resembling the clean ground truth. Key structural features, such as brain contours and fine textures, are well recovered in both cases. DnCNN shows a visible improvement over the noisy input but retains some blurring and texture loss, consistent with its lower SSIM and PSNR scores. RIDNet's output appears heavily smoothed, with many anatomical details suppressed, aligning with its poor quantitative performance. Overall, this visual analysis confirms the strong generalization of CNN-DMRI and U-Net Lite under combined noise and blur, while highlighting the limitations of RIDNet and DnCNN in handling such distortions.

TABLE V
PERFORMANCE OF RICHARDSON–LUCY

| **Condition** | **MSE** ($\times 10^{-3}$) | **SSIM** | **PSNR (dB)** |
|---|---|---|---|
| Blur only | 6.10 | 0.4946 | 23.98 |
| Blur + AWGN | 24.40 | 0.0895 | 16.18 |

Table V summarizes the performance of the Richardson–Lucy (RL) deconvolution algorithm under both clean and noisy conditions. When applied to images affected only by blur, RL achieved moderate results with an MSE of 6.10 $\times 10^{-3}$, an SSIM of 0.4946, and a PSNR of 23.98dB. These values indicate that while the method could recover basic structural content, fine details were only partially restored. Under the more challenging scenario that included additive Gaussian noise ($\sigma = 0.1$), RL performance dropped substantially: MSE rose to 24.40 $\times 10^{-3}$, SSIM fell to 0.0895, and PSNR decreased to 16.18dB. This decline highlights the algorithm's sensitivity to noise, as it lacks the adaptive learning mechanisms present in deep neural networks. Despite its simplicity, RL serves as a valuable baseline, helping to quantify the improvements gained through modern learning-based approaches.

## IV. CONCLUSIONS

This study compared four deep learning architectures—DnCNN, RIDNet, CNN-DMRI, and a lightweight U-Net variant—for the task of MRI image denoising and deblurring. Each model was evaluated under two conditions: one with synthetic blur only, and another with added Gaussian noise at $\sigma = 0.1$. A classical Richardson–Lucy (RL) deconvolution algorithm was also included as a baseline to provide context for the performance of modern approaches.

The deep learning models, particularly CNN-DMRI and U-Net Lite, consistently outperformed the RL algorithm across all evaluation metrics. While RL showed moderate capability in restoring blurred images, its performance degraded significantly in the presence of noise. In contrast, the learned models demonstrated better structural preservation, lower reconstruction error, and higher perceptual quality—even under more challenging, noisy conditions. These results confirm that fixed, hand-crafted methods like RL are limited in robustness and adaptability, whereas deep networks, trained on representative data, can generalize more effectively to complex degradation patterns.

The experimental pipeline adopted in this work ensured reproducibility and fairness through consistent preprocessing, training schedules, and evaluation metrics. All models were assessed using MSE, SSIM, and PSNR, along with visual inspection of output images and metric distributions. This comprehensive methodology helped highlight not just average performance, but also the consistency and visual fidelity of each approach.

Looking forward, deep learning techniques represent the most promising direction for robust medical image restoration. Future work should explore the integration of more advanced architectures—such as those employing attention mechanisms or transformer blocks—and examine their behavior under varying noise levels and blur conditions. Expanding evaluations to additional datasets with diverse anatomical regions and scanner settings will also be essential for ensuring generalization and clinical applicability. Overall, the results strongly support deep learning as the preferred strategy for reliable and high-quality MRI denoising in practical scenarios.

Future work could focus on extending this evaluation by introducing additional noise levels to further challenge model robustness and assess generalization under varying conditions. Exploring new or modified architectures, such as those incorporating multi-scale attention mechanisms or transformer-based designs, may yield improvements in denoising accuracy and efficiency. Additionally, testing the models across multiple MRI datasets—featuring different scanners, anatomical regions, and acquisition protocols—would offer a broader perspective on model adaptability and clinical applicability. These directions aim to enhance both the performance and reliability of deep learning methods in medical image restoration.

## REFERENCES


[1] D. L. Donoho and I. M. Johnstone, "Adapting to unknown smoothness via wavelet shrinkage," *Journal of the American Statistical Association*, vol. 90, no. 432, pp. 1200–1224, 1995.

[2] A. Buades, B. Coll, and J.-M. Morel, "A non-local algorithm for image denoising," *Proceedings of the IEEE Conference on Computer Vision and Pattern Recognition (CVPR)*, vol. 2, pp. 60–65, 2005.

[3] W. H. Richardson, "Bayesian-based iterative method of image restoration," *Journal of the Optical Society of America*, vol. 62, no. 1, pp. 55–59, 1972.

[4] L. B. Lucy, "An iterative technique for the rectification of observed distributions," *The Astronomical Journal*, vol. 79, p. 745, 1974.

[5] J. S. Lim, *Two-Dimensional Signal and Image Processing*. Prentice-Hall, Inc., 1990.

[6] K. Zhang, W. Zuo, Y. Chen, D. Meng, and L. Zhang, "Beyond a gaussian denoiser: Residual learning of deep cnn for image denoising," *IEEE Transactions on Image Processing*, vol. 26, no. 7, pp. 3142–3155, 2017.

[7] O. Ronneberger, P. Fischer, and T. Brox, "U-net: Convolutional networks for biomedical image segmentation," in *Medical Image Computing and Computer-Assisted Intervention (MICCAI)*. Springer, 2015, pp. 234–241.

[8] S. Anwar and N. Barnes, "Real image denoising with feature attention," *Proceedings of the IEEE International Conference on Computer Vision Workshops (ICCVW)*, 2019.

[9] S. W. Zamir, A. Arora, S. Khan, M. Hayat, F. S. Khan, M.-H. Yang, and L. Shao, "Multi-stage progressive image restoration," in *Proceedings of the IEEE Conference on Computer Vision and Pattern Recognition (CVPR)*, 2021, pp. 14 821–14 831.

[10] Ebtesam, "Denoised mri brain tumor datasets," https://www.kaggle.com/datasets/ebtesamkaggle/denoised-mri-brain-tumor-datasets, 2022.